Proceedings of the 21st International Conference on Global Research and Education (Inter-Academia 2024)

Assessment of the Imaging Quality of Transmissive Micro Dihedral Corner Reflectors Array

W. Finke*

Faculty of Mechatronics, Institute of Micromechanics and Photonics, Warsaw University of Technology, św. A. Boboli 8, 02-525 Warsaw, Poland

Doi: 10.12693/APhysPolA.146.457 *e-mail: weronika.finke@pw.edu.pl

A transmissive micro dihedral corner reflector array consists of numerous pairs of orthogonal surfaces that reflect light. Under such configuration, the object is imaged in mid-air with a 1:1 ratio, but with inverted depth. Despite some limitations, e.g., viewing angle, object position, or ghosting effect, the array is used for impressive 2D or 3D floating image projection. This work investigates the imaging quality of the commercially available plastic plate to quantitatively present the image deterioration. For this purpose, the set of experiments widely used for imaging optics testing is employed for a few typical arrangements. The evaluation includes resolving power, chromatic aberration, color reproduction, distortion, and uniformity.

topics: micro dihedral corner reflector array, mid-air image projection, image quality measurements

1. Introduction

The 3D displays have been of great interest for over the last 70 years. In particular, floating or mid-air image projections, which are mistakenly referred to in pop culture as holographic [1, 2], have become very firmly established in the public imagination as providing an effect of mixed reality, large angular field of view, and the possibility of interaction with the image.

For the observer, the image is most attractive when it can be perceived without the need to wear glasses or any other medium. The most sophisticated and quality method for this purpose is holography, where a high-quality wavefield is generated, however, the image size, speckle noise, and display devices are still bottlenecks of the technology [3]. Next, the light field [3, 4] is a ray-based technique that still provides high quality, but the devices are expensive and quite complex. Although there are many solutions for mid-air projections (e.g., integral imaging [5], acoustic trap [6], optical trap [7] displays, and many more [2]), in some applications, the simpler, the better. Compared to all the above, the concept of using micro-reflector arrays to produce aerial images seems to be promising [8]. The matrix of retroreflectors is used to redirect the rays back on their path, and thus the image is created. It may appear at the object plane or be redirected, depending on the micro-array structure. The image depth is pseudoscopic (inverted), but it may be implemented for 2D aerial display construction with no reverse system.

In this work, a transmissive micro dihedral corner reflector array [9] is taken under investigation. It consists of numerous pairs of orthogonal surfaces that reflect light. As a result, the image is transmitted through the plate and its direction is changed.

The goal is to adapt the methods well known from conventional imaging system testing (i.e., ISO standards TC42) to perform a test of the aerial image. The following basic properties have been chosen to be measured: uniformity (with a blank screen), color reproduction (24 patch ColorChecker), resolving power and chromatic aberration (*spatial frequency response* (SFR) of slanted knife-edge), image deformation (with a checkerboard).

2. Geometry and visual assessment

In this work, the commercially available plastic plate ASKA3D-200NT is taken under investigation. The array size is $200 \times 200 \times 6.3$ mm^3. The active layer of the thickness lower than 1 mm is sandwiched between two plastic plates. The distance between reflective layers is ≈ 600 μm (measured with the use of a workshop microscope). The plate can be used in several configurations. However, it is recommended to set the central observation angle close to $45^\circ \pm 20^\circ$. The scheme of the experimental setup is presented in Fig. 1. Reflective surfaces are arranged at 45° inclination to horizontal and vertical edges. After two reflections, the rays leave the plate on the angle $\Theta_o = -\Theta_i$, where Θ_o is the

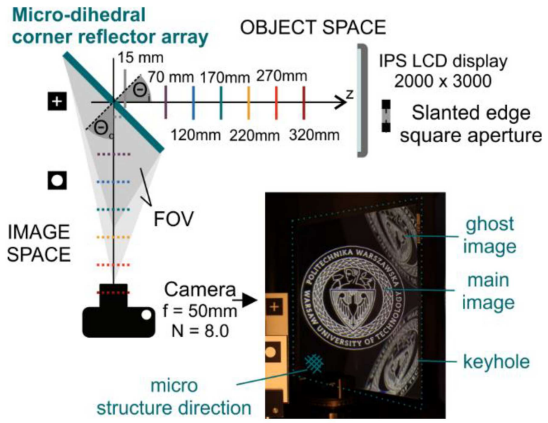

Fig. 1. The scheme of the experimental system.

output ray angle, and Θ_i is the incident ray angle. Rays which access the plate on high Θ_i pass it with a single reflection (the first or second), and therefore create two ghost images. All three component are separated angularly, so main image is overlapped with two ghost images for short distances. According to manufacturer instructions, this effect can be minimized with the use of privacy screen.

The field of view (FOV) is limited by the plate size, which works as a keyhole in holography. Therefore, the image is observed against the plate and within its surface area. FOV depends on image-to-plate distance, observer-to-image distance, and observation direction. To observe the full projected image, either the camera position needs to be changed, or the scattering medium (or screen) needs to be placed at the image plane. Image depth inversion, together with binocular disparity and limited FOV, results in slight vergence-accommodation conflict [10] while observing 3D scenes.

Due to the effects described above, the image quality at a given distance is difficult to predict, so experimental evaluation is proposed in the following chapter.

3. Image quality assessment tests

3.1. Experimental system

The proposed experimental system used for image quality assessment is presented in Fig. 1. The reflector plate is aligned to reproduce the image at the recommended 45° inclination. Object and camera move on sliders along the optical axis from $z = 15$–320 mm. Test charts are displayed with a color-calibrated, 13" IPS computer screen with a resolution of 3000 × 2000 and 247 ppi to support short recording distances. For resolving power (sharpness) tests and *modulation transfer function* (MTF) calculations, a slanted edge square aperture is used to avoid analysis failure [11]. Images are recorded with a full-frame DSLR camera of resolution 5616 × 3744 and the objective lens of focal length $f = 50$ mm and F-number of 8.0, adjusted to a focus distance of 500 mm. Images are registered in a RAW format to avoid unwanted processing of the data. Since the camera objective is subject to an aberration, as the reference, the test charts are recorded directly for the same distance and center of the image position. Ghost images prevent measurement across the entire plate for short distances, thus registration and processing schedules are adjusted. The data processing is performed with the use of MATLAB Image Acquisition and Processing Toolboxes functions.

3.2. Uniformity

The uniformity test is performed with the blank, white chart. Normalized intensity graphs with contours are presented in Fig. 2a. It is visible that brightness decreases toward the right edge of FOV, which is closer to the object (and the observer). Figure 2b presents horizontal sections of central row. For presentation purposes, all the data sets are resized and normalized to a column of 92 pix. In this visualization, the reference measurement is subtracted from captured data.

It can be seen that despite the ghost images, the trend is very similar for all the datasets. The closest image showing the intensity without ghost images is registered for distance $z = 270$ mm. In this case, the image intensity decreases from 0.99 to 0.67 from the left to the right edge ($\approx$ 120 mm distance), which gives 32%. We may approximate the intensity decrease of 2.66%/cm. However, the increasing slope inclination is noticeable; it may be the result of z distance change, camera sensitivity, or plate properties. To confirm this effect more data should be gathered with fixed camera settings.

3.3. Color reproduction

The ability of color reproduction is tested with a popular ColorChecker chart composed of 24 fields [12]. Even though the color calibration of the display is performed in advance, a slight color error is still present in the experimental chart registered directly with the use of the camera. Therefore, color patches do not correspond precisely to the original ColorChecker chart values. Color reproduction errors ΔE are also calculated in relation to the experimental chart. Exposure time was adjusted to compensate for the brightness decrease on transmission through the plate. In Fig. 3a, a visual color comparison and color errors ΔE are shown. Each color patch represents the measured color, and the frame is the reference color.

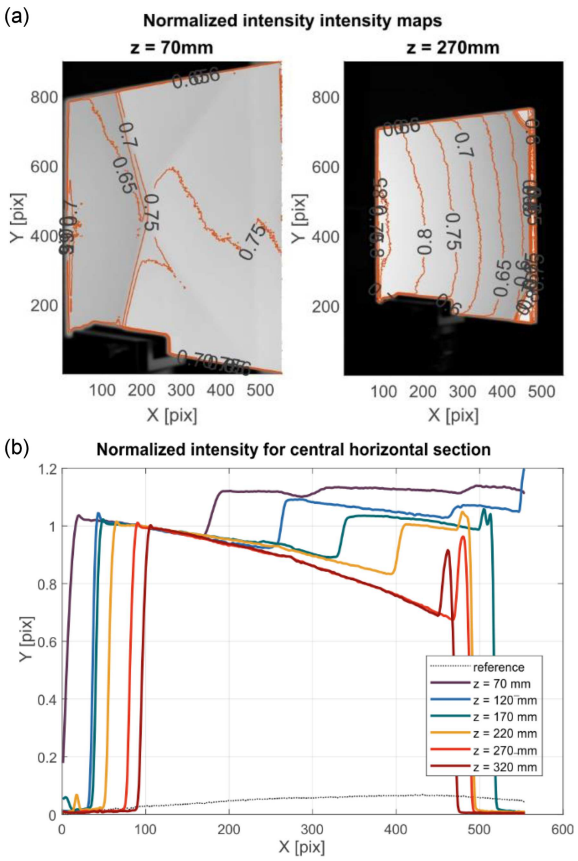

Fig. 2. Uniformity analysis: (a) exemplary normalized intensity maps for distances $z = 70$ mm and $z = 270$ mm, (b) normalized intensity for the central horizontal section for all the registered distances.

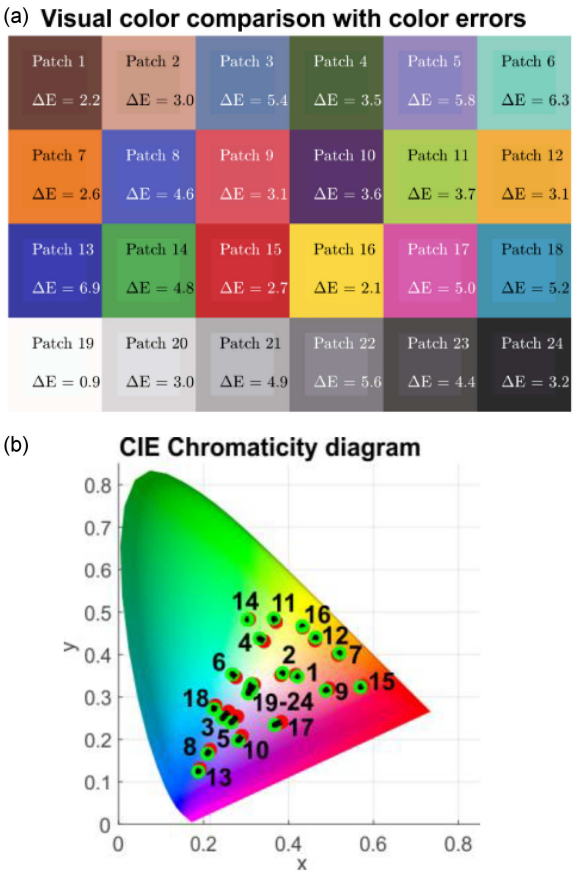

Fig. 3. Color reproduction test result: (a) visual color comparison with errors, (b) CIE chromaticity diagram.

The closer to the value of 1, the lower the color difference. In this case, the color error stays almost within the range for prints (3 to 6). The maximum value $\Delta E = 6.9$ is present for Patch 13, while the average error is 3.98. The CIE chromaticity diagram confirms good color reproduction (red points are references, and green points are measured values).

3.4. Image deformation

Image deformation is observed with the use of a checkerboard chart, commonly used for distortion measurements [13]. The size of the checkerboard was selected to match at least 5 fields in the row for the furthest image position. Each field is a square of 11×11 mm^2. Exemplary images are presented in Fig. 4. Since strong skewing and sharpness decrease is present in the image, it is difficult to calculate the distortion. Therefore, here the angle of inclination for horizontal α and vertical β edges is indicated and presented in Table I.

TABLE I

Image skew angle for horizontal and vertical edges at a distance of z.

Distance z [mm]	Angle of skew	
	Horizontal α	Vertical β
70	0.69°	−0.72°
120	1.11°	−0.87°
170	1.49°	−1.64°
220	1.75°	−1.86°
270	2.21°	−2.69°
320	2.66°	−3.40°

According to the obtained data, a skew angle is higher for the horizontal and vertical directions of the image. The average skew in the horizontal direction is 0.087°/cm and 0.094°/cm in the vertical direction. Moreover, precise corner indication is difficult due to blur, chromatic aberration, and image waving. Therefore, image deformation tests require a more advanced image processing algorithm. The dot pattern should be considered as more resistant

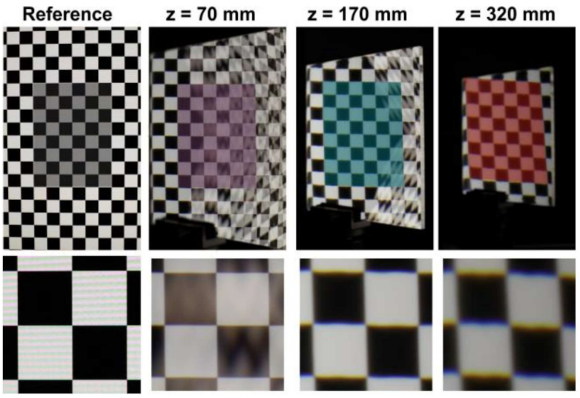

Fig. 4. Exemplary checkerboard images (and details for reference) and exemplary distances.

to sharpness loss. Finally, since the image is not circularly symmetrical, a deformation map would provide supplementary information.

3.5. Sharpness and chromatic aberration

Sharpness (resolving power) and chromatic aberration are calculated based on the slanted edge test, which is the most suitable pattern to minimize errors introduced by digital sensors [14]. It is not recommended to use a pixelated display as the chart, so the square aperture of size 6×6 mm^2 is used. The image is characterized by the use of the spatial frequency response (SFR) function, which measures the ability to reproduce fine details across a range of spatial frequencies [11, 15]. To compare results for different distances, the modulation transfer function (MTF) is used. It describes a relative contrast in a given spatial frequency. The most widely used parameter is MTF50, where MTF is equal to 50% of the low-frequency contrast. Images of the aperture and region of interest (ROI) arrangement are presented in Fig. 5a. Most rapid image sharpness loss (Fig. 5b) is observed for short distances, where average MTF50 decreases from 26.66 LP/mm to 7.53 LP/mm between reference and shortest possible distance to be measured (15 mm), to reach 2.33 LP/mm for 170 mm. The trend is similar for all the ROIs. It must be noticed that, in this case, chromatic aberration, together with skewing and edge waving effects, will affect the SFR results. More samples should be processed to confirm the trends.

With the use of the same dataset, a chromatic aberration is measured. It is defined as the area between maximum and minimum red, green, and blue edge intensity profiles (see Fig. 5c). It increases with distance, and horizontal edges are over 3 times more aberrated than vertical ones.

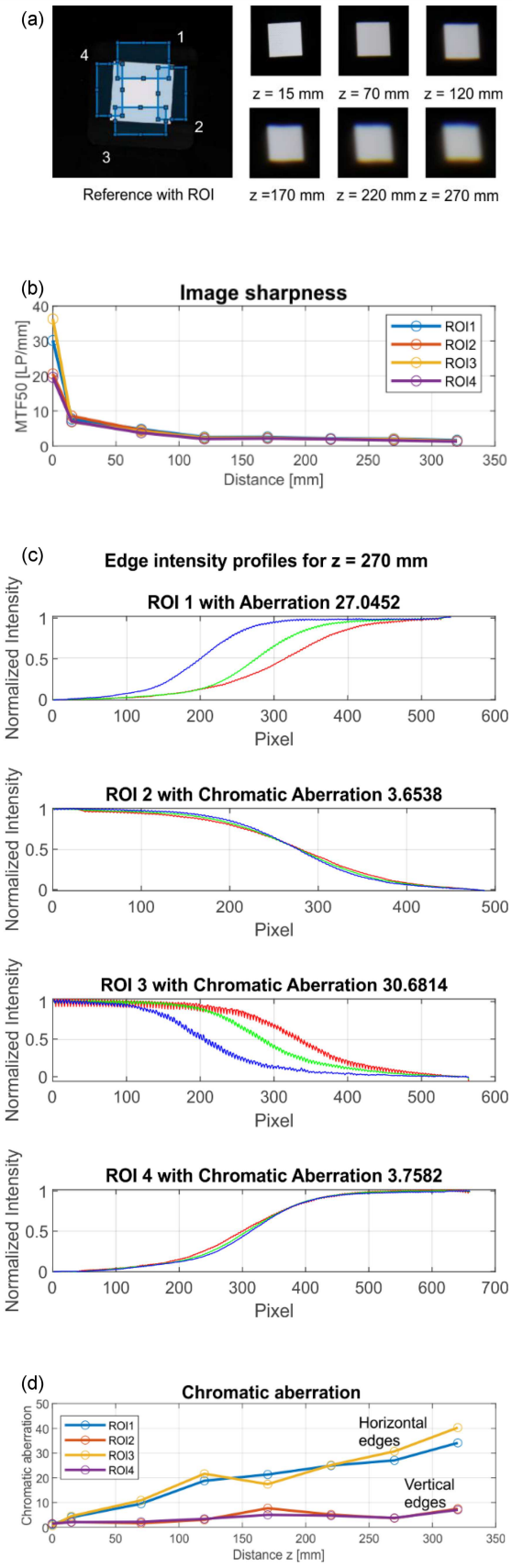

Fig. 5. Sharpness and chromatic aberrations tests: (a) registered data, (b) image sharpness (MTF50), (c) exemplary (z = 270 mm) RGB edge intensity profiles for a given ROI, (d) chromatic aberration.

4. Conclusions

This work presents an attempt to evaluate a non-conventional imaging device, i.e., micro dihedral corner reflector array, with the use of methods widely used in photography. However, although the main limitations are indicated, the accuracy and precision tests need to be performed to confirm the values obtained in these experiments. Below, five investigated aspects are summed up.

First, the image brightness decreases toward the shorter object distances (here — right edge). We may approximate the intensity decrease of 2.66%/cm in the horizontal direction. The slope of the profile slightly increases with the distance, but to confirm this effect more data should be gathered with fixed camera settings.

Second, color reproduction is very good. The maximum error $\Delta E = 6.9$ is slightly above the strict print requirements (range 3–6). However, considering the uniformity test, the intensity decrease within the test chart area is higher than 20%, which may be the source of error. Therefore, the sequential color display is recommended.

Third, the most noticeable image deformation is the skewing proportional to the object distance. The average skew in the horizontal direction is 0.087°/cm and 0.094°/cm in the vertical direction. However, the image deformation is complex, and more advanced analysis needs to be performed. The checkerboard chart is difficult to process due to image quality loss and non-circularly symmetrical image deviation. Under such conditions, a less sharpness-sensitive chart, e.g., dot pattern and deformation map, would provide supplementary information.

Fourth, image sharpness most rapidly decreases for short distances. This means that in the presented configuration, the image quality will vary from the left to right side of the FOV. Assuming the closest to plate object position, the right edge distance is 15 mm, and the left edge distance is 155 mm, so according to the recorded data, in the best case, the MTF50 parameter varies from 7.5 to 2.5 LP/mm. In general, the slanted knife-edge test works well with this type of data, however, due to the skewing effect and chromatic aberration, the test angle needs to be adjusted, and focus indication is problematic even for short depths of field.

Fifth, chromatic aberration, as all the above effects, increases with the distance. It is almost 3 times more steep for horizontal than for vertical edges. However, based on the provided results, it is not clear what is the azimuth of maximum aberration. Therefore, the dot pattern would provide supplementary information as well as image deformation tests.

Summing up, the image quality assessment methods well known from conventional imaging system testing can be adapted for the aerial image test, but with certain restrictions. First, due to the quality variation across the field of view, the local or sequential tests within the limited area should be performed if possible (slanted edge, color reproduction). Second, high image sharpness loss does not allow for edge or corner recognition (checkerboard should be substituted with a dot pattern). Third, the image deterioration is complex and should not be angularly limited to horizontal and vertical directions (chromatic aberration, image deformation). Fourth, appropriate camera settings may support further processing. For example, short depth of field supports differentiation between main and ghost images.

The restrictions presented above should be included in future works.

References

[1] G.T. Nehmetallah, R. Aylo, L. Williams, in: *Analog and Digital Holography with MATLAB*, 2015, Ch. 11, p. 411.

[2] J. Geng *Adv. Opt. Photon.* **5**, 456 (2013).

[3] M. Yamaguchi, *J. Opt. Soc. Am. A* **33**, 2348 (2016).

[4] M. Levoy, P. Hanrahan, in: *Proc. 23rd Int. Conf. on Computer Graphics and Interactive Techniques (SIGGRAPH 1996)*, 1996.

[5] W.X. Zhao, H.L. Zhang, Q.L. Ji, H. Deng, D.H. Li, *Photonics* **8**, 381 (2021).

[6] R. Hirayama, D. Martinez Plasencia, N. Masuda, S. Subramanian, *Nature* **575** 320, (2019).

[7] D.E. Smalley, E. Nygaard, K. Squire et al., *Nature* **553**, 486 (2018).

[8] Y. Terashima, S. Suyama, H. Yamamoto, *Opt. Rev.* **26**, 179 (2019).

[9] M. Otsubo, *Proc. Int. Disp. Work.* **28**, 227 (2021).

[10] D.M. Hoffman, A.R. Girshick, K. Akeley, M.S. Banks, *J. Vis.* **8**, 33 (2008).

[11] P.D. Burns in: *Society for Imaging Science and Technology: Image Processing, Image Quality, Image Capture, Systems Conference (PICS 2000)*, 2000, p. 135.

[12] D. Pascale, RGB coordinates of the Macbeth ColorChecker, The BabelColor Company, 2006.

[13] J. Weng, P. Cohen, M. Herniou, *IEEE Trans. Pattern Anal. Mach. Intell.* **14**, 965 (1992).

[14] K. Parulski, D. Wueller, P. Burns, H. Yoshida, in: *Int. Symp. Electronic Imaging (IA 2022)*, 2022, p. 347.

[15] N. Kawagishi, R. Kakinuma, H. Yamamoto, *Opt. Express* **28**, 35518 (2020).